AIP | Review of Scientific Instruments

Theoretical and experimental study of the dynamic response of absorber-based, micro-scale, oscillatory probes for contact sensing applications

Sajad Kafashi, Ralph Strayhorn, Jeff D. Eldredge, Scott D. Kelly, Shane C. Woody, and Stuart T. Smith

Citation: Review of Scientific Instruments **87**, 065005 (2016); doi: 10.1063/1.4954164
View online: http://dx.doi.org/10.1063/1.4954164
View Table of Contents: http://scitation.aip.org/content/aip/journal/rsi/87/6?ver=pdfcov
Published by the AIP Publishing

REVIEW OF SCIENTIFIC INSTRUMENTS **87**, 065005 (2016)

Theoretical and experimental study of the dynamic response of absorber-based, micro-scale, oscillatory probes for contact sensing applications

Sajad Kafashi,[1,a)] Ralph Strayhorn,[1] Jeff D. Eldredge,[2] Scott D. Kelly,[3] Shane C. Woody,[4] and Stuart T. Smith[1]
[1]*Center for Precision Metrology at UNC Charlotte, Charlotte, North Carolina 28223, USA*
[2]*Mechanical and Aerospace Engineering, University of California, Los Angeles, Los Angeles, California 90095, USA*
[3]*Mechanical Engineering and Engineering Science, UNC Charlotte, Charlotte, North Carolina 28223, USA*
[4]*InsituTec Inc., 7140 Weddington Road Suite 144, Concord, North Carolina 28027, USA*

(Received 24 February 2016; accepted 4 June 2016; published online 22 June 2016)

This paper presents two models for predicting the frequency response of micro-scale oscillatory probes. These probes are manufactured by attaching a thin fiber to the free end of one tine of a quartz tuning fork oscillator. In these studies, the attached fibers were either 75 μm diameter tungsten or 7 μm diameter carbon with lengths ranging from around 1 to 15 mm. The oscillators used in these studies were commercial 32.7 kHz quartz tuning forks. The first theoretical model considers lateral vibration of two beams serially connected and provides a characteristic equation from which the roots (eigenvalues) are extracted to determine the natural frequencies of the probe. A second, lumped model approximation is used to derive an approximate frequency response function for prediction of tine displacements as a function of a modal force excitation corresponding to the first mode of the tine in the absence of a fiber. These models are used to evaluate the effect of changes in both length and diameter of the attached fibers. Theoretical values of the natural frequencies of different modes show an asymptotic relationship with the length and a linear relationship with the diameter of the attached fiber. Similar results are observed from experiment, one with a tungsten probe having an initial fiber length of 14.11 mm incrementally etched down to 0.83 mm, and another tungsten probe of length 8.16 mm incrementally etched in diameter, in both cases using chronocoulometry to determine incremental volumetric material removal. The lumped model is used to provide a frequency response again reveals poles and zeros that are consistent with experimental measurements. Finite element analysis shows mode shapes similar to experimental microscope observations of the resonating carbon probes. This model provides a means of interpreting measured responses in terms of the relative motion of the tine and attached fibers. Of particular relevance is that, when a "zero" is observed in the response of the tine, one mode of the fiber is matched to the tine frequency and is acting as an absorber. This represents an optimal condition for contact sensing and for transferring energy to the fiber for fluid mixing, touch sensing, and surface modification applications. *Published by AIP Publishing.* [http://dx.doi.org/10.1063/1.4954164]

I. INTRODUCTION

Tuning fork and other quartz-based oscillators are commonly used as timers in clocks, AFM probes,[1–4] touch sensitive sensors, micro-robotics fingers,[5–7] and micro balances.[8] Micro-scale oscillatory probes made by attaching carbon, glass, or tungsten fibers to a quartz tuning fork tine provide a capability to both oscillate the fiber and monitor changes in its response when the fiber comes into proximity with external objects or is immersed in fluids. These probes have been used for a broad range of applications including for surface modification studies in vortex machining process,[9–11] touch probes in coordinate measuring machines (CMMs),[6] touch-sensitive micro-robotic fingers,[5] and in high speed fluid-flow in microfluidics studies.[12] Another study plans to use these tuning fork-based micro probes for investigation on micro-particles dynamics around dynamically vibrating objects for non-contact manipulation of particles immersed in fluids, which can be used for assembly and sorting/shepherding particles.[13–16]

To better control these processes, it is necessary to interpret the measured responses of the probes in terms of the fiber and tuning fork dynamics. Hence a mathematical model of oscillating fibers attached to a tuning fork tine is provided in this article. This will be represented in two main sections, the theory behind the two serially connected beams model and the lumped absorber model, results from which are compared with experimental data and finite element analysis (FEA).

II. THEORY

In most of the micro-probe applications, a tuning fork is used as an oscillation mechanism to drive a fiber attached to

[a)]Author to whom correspondence should be addressed. Electronic mail: skafashi@uncc.edu.

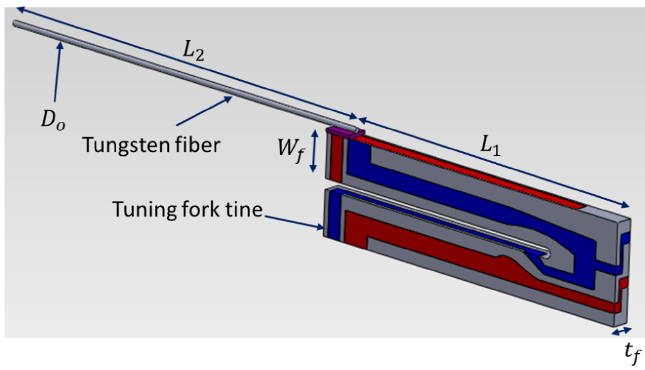

FIG. 1. Model of tuning fork with a tungsten fiber attached to its upper tine showing the critical dimensional parameters used for vibration analysis of the probe system.

it. This section presents two vibration models of the tuning fork-based probes one is two Euler-beams serially connected and the other is a simplified lumped model approximation. A 3D solid model of a 75 μm diameter tungsten fiber attached to a tuning fork tine with the important geometric parameters is shown in Figure 1.

The blue and red regions in the model represent the electrodes to which an oscillating potential difference is applied.

A. Lateral vibration of two beams serially connected

Using the Euler beam equation,[17] mode shapes for these two beams are given by

$$\frac{y_1(x_1,q_1)}{q_1} = A_1\cos(\alpha_1 x_1) + A_2\cosh(\alpha_1 x_1) + A_3\sin(\alpha_1 x_1) + A_4\sinh(\alpha_1 x_1), \quad (1)$$

$$\frac{y_2(x_2,q_2)}{q_2} = B_1\cos(\alpha_2 x_2) + B_2\cosh(\alpha_2 x_2) + B_3\sin(\alpha_2 x_2) + B_4\sinh(\alpha_2 x_2), \quad (2)$$

$$\alpha_1^4 = \frac{m_1}{L_1E_1I_1}\omega_s^2, \alpha_2 = \frac{m_2}{L_2E_2I_2}\omega_s^2.$$

The parameters y_1 and y_2 are the lateral deflections of the tuning fork tine and fiber as a function of axial distances x_1 and x_2 measured from the fixed end, respectively. Additionally, parameters m, E, L, and I represent the mass, elastic modulus, length, and second moment of area about the neutral axis of bending with subscripts 1 and 2 representing the tuning fork tine and the fiber, respectively. To determine mode shapes and natural frequencies, it is necessary that the above equations satisfy the eight boundary conditions (a)–(f)

$$\begin{aligned}
&(a)\ y_1 = \left.\frac{dy_1}{dx_1}\right|_{x_1=0} = 0,\\
&(b)\ y_1|_{x_1=L_1} = y_2|_{x_2=0},\\
&(c)\ \left.\frac{dy_1}{dx_1}\right|_{x_1=L_1} = \left.\frac{dy_2}{dx_2}\right|_{x_2=0},\\
&(d)\ E_1I_1\left.\frac{d^2y_1}{dx_1^2}\right|_{x_1=L_1} = E_2I_2\left.\frac{d^2y_2}{dx_2^2}\right|_{x_2=0},\\
&(e)\ E_1I_1\left.\frac{d^3y_1}{dx_1^3}\right|_{x_1=L_1} = E_2I_2\left.\frac{d^3y_2}{dx_2^3}\right|_{x_2=0},\\
&(f)\ \frac{d^2y_2}{dx_2^2} = \left.\frac{d^3y_2}{dx_2^3}\right|_{x_2=L_2} = 0.
\end{aligned} \quad (3)$$

From the first of these conditions, Equations (1) and (2) can be rearranged in a simplified form

$$\frac{y_1(x_1,q_1)}{q_1} = A_1(\cos(\alpha_1 x_1) - \cosh(\alpha_1 x_1)) + A_3(\sin(\alpha_1 x_1) - \sinh(\alpha_1 x_1)), \quad (4)$$

$$\frac{y_2(x_2,q_2)}{q_2} = B_1\cos(\alpha_2 x_2) + B_2\cosh(\alpha_2 x_2) + B_3\sin(\alpha_2 x_2) + B_4\sinh(\alpha_2 x_2). \quad (5)$$

To solve for the natural frequency of this combined system it is necessary to express the α coefficients in terms of a common eigenvalue form

$$\omega_s^2 = (\alpha_{s1}L_1)^4\frac{E_1I_1}{\rho_1A_1L_1^4} = (\alpha_{s1}L_1)^4\frac{E_1I_1}{m_1L_1^3} = (\alpha_{s2}L_2)^4\frac{E_2I_2}{m_2L_2^3}, \quad (6)$$

$$(\alpha_{s1}L_1)^4 = (\alpha_{s2}L_2)^4\frac{m_1L_1^3}{m_2L_2^3}\frac{E_2I_2}{E_1I_1} = (\alpha_{s2}L_2)^4\lambda\kappa = \beta^4(\alpha_{s2}L_2)^4, \quad (7)$$

$$\gamma = \frac{L_2}{L_1}, \varphi = \alpha_2L_2, \quad (8)$$

$$\alpha_{s1} = \beta\frac{L_2}{L_1}, \alpha_{s2} = \beta\gamma\alpha_{s2}. \quad (9)$$

The description of these parameters and their values in the model are given in Tables II and III. In Equation (6), the subscript s represents the modal frequency. It is important to note that the constant β is a function only of the materials and geometry of the fiber and tine. Appendix details the derivation of the equations of this section.

Equations (A3)–(A7) (provided in the Appendix) can be written in matrix form

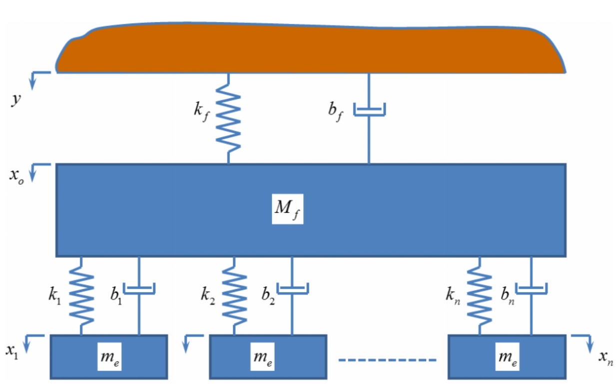

FIG. 2. Lumped absorber model of the fiber probe.

$$\begin{bmatrix} \cos(\beta\alpha_2 L_2) - \cosh(\beta\alpha_2 L_2) & \sin(\beta\alpha_2 L_2) - \sinh(\beta\alpha_2 L_2) & -1 & -1 & 0 & 0 \\ -\beta\gamma(\sin(\beta\alpha_2 L_2) + \sinh(\beta\alpha_2 L_2)) & \beta\gamma(\cos(\beta\alpha_2 L_2) - \cosh(\beta\alpha_2 L_2)) & 0 & 0 & -1 & -1 \\ -E_1 I_1 (\beta\gamma)^2(\cos(\beta\alpha_2 L_2) + \cosh(\beta\alpha_2 L_2)) & -E_1 I_1 (\beta\gamma)^2(\sin(\beta\alpha_2 L_2) + \sinh(\beta\alpha_2 L_2)) & E_2 I_2 & -E_2 I_2 & 0 & 0 \\ E_1 I_1 (\beta\gamma)^3(\sin(\beta\alpha_2 L_2) - \sinh(\beta\alpha_2 L_2)) & -E_1 I_1 (\beta\gamma)^3(\cos(\beta\alpha_2 L_2) + \cosh(\beta\alpha_2 L_2)) & 0 & 0 & E_2 I_2 & -E_2 I_2 \\ 0 & 0 & -\cos(\alpha_2 L_2) & \cosh(\alpha_2 L_2) & -\sin(\alpha_2 L_2) & \sinh(\alpha_2 L_2) \\ 0 & 0 & \sin(\alpha_2 L_2) & \sinh(\alpha_2 L_2) & -\cos(\alpha_2 L_2) & \cosh(\alpha_2 L_2) \end{bmatrix} \begin{Bmatrix} A_1 \\ A_3 \\ B_1 \\ B_2 \\ B_3 \\ B_4 \end{Bmatrix} = \{\mathbf{0}\}. \tag{10}$$

Substituting $\psi_s = \alpha_{s2} L_2$ and $s = 1, 2, \ldots, \infty$ Equation (10) can be expressed as

$$\begin{bmatrix} \cos(\beta\psi_{s2}) - \cosh(\beta\psi_{s2}) & \sin(\beta\psi_{s2}) - \sinh(\beta\psi_{s2}) & -1 & -1 & 0 & 0 \\ -\beta\gamma(\sin(\beta\psi_{s2}) + \sinh(\beta\psi_{s2})) & \beta\gamma(\cos(\beta\psi_{s2}) - \cosh(\beta\psi_{s2})) & 0 & 0 & -1 & -1 \\ -(\beta\gamma)^2(\cos(\beta\psi_{s2}) + \cosh(\beta\psi_{s2})) & -(\beta\gamma)^2(\sin(\beta\psi_{s2}) + \sinh(\beta\psi_{s2})) & \kappa & -\kappa & 0 & 0 \\ (\beta\gamma)^3(\sin(\beta\psi_{s2}) - \sinh(\beta\psi_{s2})) & -(\beta\gamma)^3(\cos(\beta\psi_{s2}) + \cosh(\beta\psi_{s2})) & 0 & 0 & \kappa & -\kappa \\ 0 & 0 & -\cos(\psi_{s2}) & \cosh(\psi_{s2}) & -\sin(\psi_{s2}) & \sinh(\psi_{s2}) \\ 0 & 0 & \sin(\psi_{s2}) & \sinh(\psi_{s2}) & -\cos(\psi_{s2}) & \cosh(\psi_{s2}) \end{bmatrix} \begin{Bmatrix} A_1 \\ A_3 \\ B_1 \\ B_2 \\ B_3 \\ B_4 \end{Bmatrix} = \{\mathbf{0}\}. \tag{11}$$

A Matlab™ program is used to find the eigenvalues of this matrix for given κ, β, and γ. The length of the fiber is varying by etch increment in the program, and the obtained eigenvalues (ψ_{s2}) of matrix in Equation (11) are the natural frequencies of the system, representing different modal frequencies of the probe at each fiber length.

B. Lumped absorber model

Generally, the tuning fork tine is excited with an applied distortion characteristic of the first mode shape for lateral vibration in the plane of the two tines. Theoretically, an excitation force distributed along the tine corresponding to this mode shape will excite only modes with single node lateral deflection. Because the system to be modeled comprises the tuning fork tine with a relatively small fiber attached (in practice, with a small amount of epoxy adhesive) at the free end, to a first approximation, the tine can be modeled as a single degree of freedom system. Assuming that the attached fiber has a little influence on the tine, it is reasonable to expect that the fiber will only have major significance on the tine response if the modes of the fiber are correspondingly close to that of the tine. Indeed, if the fiber attached to the tine has a coincident eigenvalue, it can act as an absorber. To understand the expected behavior of a fiber probe as a function of fiber dimensions (later evaluated using electrochemical etching), a lumped model of the complete probe system is shown in Figure 2.

The various parameters of this model are given in Table I.

Generally, values for the equivalent stiffness and mass of the fiber elements are chosen to result in similar modal frequencies. Damping coefficients are more difficult to assess. For tuning fork tines in air, experience shows Q values ranging from a few hundred up to a few thousand. The fibers are near to ideal being essentially bonded to the ends of the tines and extending freely. Hence a low value for the intrinsic modal damping has been assumed. For simplification of computing, each mode is assumed to have a similar damping ratio for which free vibration exponential decay will be proportional to the modal frequency (i.e., damping proportionate to stiffness in modal analysis models).[18]

For the tuning fork tine undergoing a first mode oscillation, Rayleigh's method produces a reasonable estimate of the natural frequency. For this method the Rayleigh's quotient can be derived by assuming a deflection shape corresponding to the deflection of the beam due to a load at the free end. In this case, the stiffness at this free end, k_f, can be derived from the equation

$$k_f = \frac{3E_f I_f}{L_f^3}, \tag{12}$$

$$I_f = \frac{w_f t_f^3}{12}.$$

All symbols and their values used for theoretical calculation are defined in Table II. Additionally, it is known that the tuning fork in its free state (i.e., with no fiber attached) has a defined first mode frequency typically around 32 kHz (or 40 kHz in some cases). Hence, its representation as a single degree of freedom system can be represented by the lumped equation from which its free-state, undamped natural frequency, ω_f, can be expressed as

$$\omega_f^2 = \frac{k_f}{M_f}. \tag{13}$$

TABLE I. Descriptions of mathematical parameters shown in Figure 2 and their units.

Description	Symbols	Units
Tuning fork tine equivalent mass	M_f	kg
Tuning fork tine equivalent stiffness	k_f	N m^{-1} or kg s^{-2}
Tuning fork tine equivalent damping	b_f	N s m^{-1} or kg s^{-1}
Fiber modal mass	m_i $i = 1, \ldots, n$	kg
Fiber modal stiffness	k_i $i = 1, \ldots, n$	N m^{-1} or kg s^{-2}
Fiber modal damping	b_i $i = 1, \ldots, n$	N s m^{-1} or kg s^{-1}
Tuning fork excitation	y	m
Number of modes used in lumped model	n	1

TABLE II. Description of tuning fork parameters used in equations to determine values for the parameters of the lumped model and serially connected beams analysis, and their values used for images represented in the result section.

Description	Parameter	Value in model	Units
Width of the tuning fork tine	W_f	0.0008	m
Thickness of the tuning fork tine	t_f	0.0004	m
Length of the tuning fork tine	L_f	0.004	m
Quartz elastic modulus	E_f	75	GPa
Second moment of area of tuning fork	I_f	$\frac{1}{12} W_f t_f^3$	m^4
Damping ratio of tuning fork tine	ξ_f	0.001	(dimensionless)
Damping coefficient for tuning fork tine	b_f	$2\xi_f\sqrt{k_f M_f}$	N s m^{-1}
Equivalent mass of tuning fork tine	M_f	$\frac{k_f}{\omega_f^2}$	kg
Tuning fork tine stiffness	k_f	$\frac{E_f W_f t_f^3}{4L_f^3}$	N m^{-1}
Density of tuning fork tine	ρ_f	2620	kg m^{-3}

For a given free state natural frequency the above equation can be rearranged to give an expression for the equivalent lumped mass. Based on these values, the damping coefficient of the system is readily given by

$$b_f = 2\xi_f\sqrt{k_f M_f}. \tag{14}$$

In all cases x represents the modal coordinate for displacement at the free end. For the fiber, each mode is represented by a single degree of freedom system with energy storage and dissipation elements. Equating the elements of the individual modes with a discrete lumped mass it is reasonable to assume that a system in which at the extreme stiffness values will converge to a lumped system of comprising the tine plus total fiber mass. From a modal equation for the fiber as a cantilever independent of the tine (this will occur when the fiber is acting as a perfect absorber), it is found that the modal mass is constant for each modal coordinate while the stiffness will increase in proportion to the eigenvalue. Based on these assumptions, the lumped parameters can be obtained from the eigenvalues given by

TABLE IV. The first ten roots for lateral natural frequencies of a free cantilever beam.

Frequency r	$(\alpha\mu_r l)$
1	1.875 104 068 73
2	4.694 091 133
3	7.854 757 438 2
4	10.995 540 742
5	14.137 168 391
6	17.278 759 532 085
7	20.420 352 251 041
8	23.561 944 901 806 4
9	26.703 537 555 518 3
10	29.845 130 209 102 88

$$\lambda_i^2 = (\alpha_i L)^4 \frac{EI}{\rho A L^4}. \tag{15}$$

Therefore,

$$k_i = (\alpha_i L)^4 \frac{EI}{nL^3},\ m_e = \rho AL/n,\ b_i = 2\xi_i\sqrt{k_i m_e}. \tag{16}$$

Two different fibers, i.e., carbon and tungsten are used in the experiments for comparison with the theoretical results (represented in Section IV). The description of two fiber parameters and their values used in theoretical calculation are given in Table III.

The root $(\alpha_i L)$ are obtained from the boundary conditions of the beam. For a free cantilever, these roots for the first ten modes are given in Table IV. Due to the slow convergence of modal series and sensitivity to small variations in constants of subsequent simulations, the number of significant digits provided in this table is often necessary for modal analysis.

Equations (12)–(16) provide the necessary relationships between the probe assembly and lumped model. The dissipation function, D, potential, U, and kinetic energy, T, for the lumped model in Figure 2 are given by

$$D = \frac{1}{2} b_f (\dot{x}_o - \dot{y})^2 + \frac{1}{2}\sum_{i=1}^{n} b_i (\dot{x}_i - \dot{x}_o)^2,$$

TABLE III. Description of carbon and tungsten fiber parameters used in equations to determine values for the parameters of the lumped model and serially connected beams analysis, and their values used for calculation represented in Section IV.

Description	Parameter	Value in model, tungsten	Value in model, carbon	Units
Density of fiber	ρ	19250	2250	kg m^{-3}
Damping ratio of fiber	ξ_i	0.000 001	0.000 001	(dimensionless)
Damping coefficient of fiber for ith mode	b_i	$2\xi_i\sqrt{k_i m_e}$	$2\xi_i\sqrt{k_i m_e}$	N·s·m^{-1}
Fiber diameter	D_o	75	7	μm
Equivalent mass of fiber	m_e	ρAL	ρAL	kg
Etched length of fiber	L	Varying	Varying	m
Area of fiber	A	$\pi\frac{D_o{}^2}{4}$	$\pi\frac{D_o{}^2}{4}$	m^2
Elastic modulus of fiber	E	411	235	GPa
Second moment of area of fiber	I	$\pi\frac{D_0{}^4}{64}$	$\pi\frac{D_0{}^4}{64}$	m^4

$$U = \frac{1}{2}k_f(x_o - y)^2 + \frac{1}{2}\sum_{i=1}^{n} k_i(x_i - x_o)^2, \tag{17}$$

$$T = \frac{1}{2}M_f\dot{x}_o^2 + \frac{m_e}{2}\sum_{i=1}^{n}\dot{x}_i^2.$$

Lagrange equation provided below is used to obtain the equations governing motion for the model. Therefore equations in (17) are substituted in the Lagrange equation,[17–19]

$$\frac{d}{dt}\frac{\partial T}{\partial \dot{q}_i} - \frac{\partial T}{\partial q_i} + \frac{\partial D}{\partial \dot{q}_i} + \frac{\partial U}{\partial q_i} = 0. \tag{18}$$

Correspondingly, the equations governing motion of this system are given by

$$M_f\ddot{x}_0 + \left(b_f + \sum_{i=1}^{n} b_i\right)\dot{x}_o + \left(k_f + \sum_{i=1}^{n} k_i\right)x_o + \sum_{i=1}^{n} k_i x_i - \sum_{i=1}^{n} b_i\dot{x}_i = b_f\dot{y} + k_f y \tag{19}$$

$$[m_e\ddot{x}_i + b_i(\dot{x}_i - \dot{x}_o) + k_i(x_i - x_o) = 0]$$
$$(i = 1, \ldots, n).$$

Figure 3 is a linear system diagram relating the output displacement of each coordinate for which y is the displacement generated by the input electrical voltage that causes a static deflection closely approximating the shape of the first mode of the tuning fork tine. x_o represents the displacement of the tuning fork tine, and x_i represents the displacement of the fiber in its i-th mode. The steady stated frequency responses of the individual coordinates of this system can be obtained using the assumed solutions

$$\begin{aligned} y &= Ae^{j\omega t},\\ x_o &= H_{oy}(j\omega)y,\\ x_i &= H_{iy}(j\omega)y. \end{aligned} \tag{20}$$

Substituting (20) into (19) and rearranging yield an expression for the steady state frequency response at coordinates x given by

$$H_{oy}(j\omega) = \frac{x_o}{y} = \frac{k_f + j\omega b_f}{\left[-M_f\omega^2 + j\omega\left(b_f + \sum_{i=1}^{n} b_i\right) + \left(k_f + \sum_{i=1}^{n} k_i\right)\cdots - \sum_{i=1}^{n}\left\{\frac{k_i + j\omega b_i\left(1 + j2\xi_i\frac{\omega}{\lambda_i}\right)}{\left(1 - \frac{\omega^2}{\lambda_i^2}\right) + j2\xi_i\frac{\omega}{\lambda_i}}\right\}\right]}, \tag{21}$$

$$H_{iy}(j\omega) = \frac{x_i}{y} = \left\{\frac{k_i + j\omega b_i\left(1 + j2\xi_i\frac{\omega}{\lambda_i}\right)}{\left(1 - \frac{\omega^2}{\lambda_i^2}\right) + j2\xi_i\frac{\omega}{\lambda_i}}\right\} H_{oy}(j\omega). \tag{22}$$

A Matlab code is developed to compute these frequency response functions as the fiber length is shortened. In practice for a tuning fork based probe, it will be the tine displacement that is sensed and therefore will be measured as the frequency response of the probe, see Section IV C.

III. OVERVIEW OF EXPERIMENTAL APPROACH

Fiber probes are fabricated by manually aligning the fiber and tuning fork tine under an optical microscope using a multi-axis micrometer driven stage. Once aligned the tungsten and carbon fibers are attached by high strength epoxy (Norland optical adhesive #61). Figure 4 shows a 75 μm diameter tungsten fiber glued to the upper tine of a quartz tuning fork.

An electrochemical etching apparatus is used for precise material removal for the purpose of controlled shortening of the length or diameter reduction of the fiber. The etching

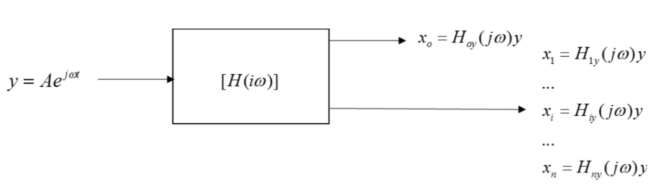

FIG. 3. Input-output linear system model. For the probe demonstration.

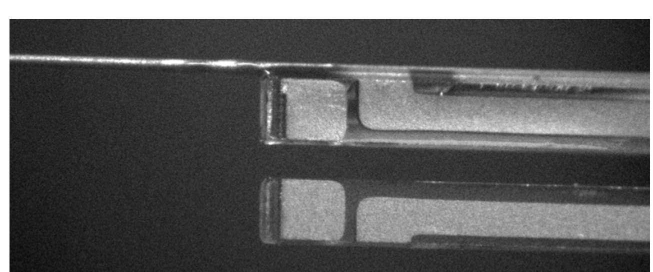

FIG. 4. Photograph of 75 μm diameter tungsten fiber attached to the upper tine of tuning fork along with the tine axis.

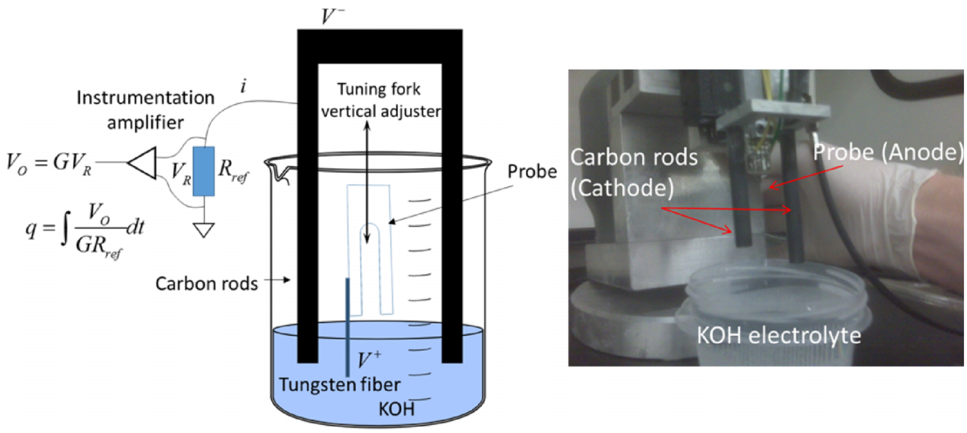

FIG. 5. An image of etching apparatus used for mass removal of fibers. A voltage applied across the carbon rods (cathode) and tungsten fiber (anode) that creates a current through the electrolyte that is measured to calculate the mass removal.

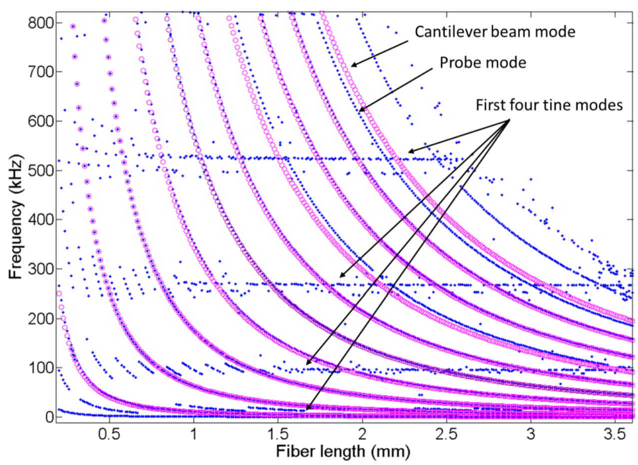

FIG. 6. Theoretical calculation of frequency as a function of length of fiber for first ten resonant modes obtained from theoretical model for two serially connected beams (carbon probe).

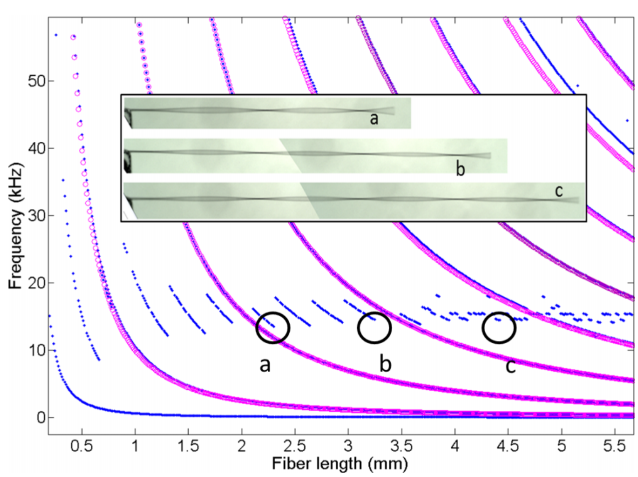

FIG. 7. Three visible modes of carbon fiber with 7 μm diameter, (a) third mode with length 2.4 mm, (b) fourth mode with length 3.3 mm, and (c) fifth mode with length 4.3 mm. The theory model predicts these lengths when the natural frequencies of fiber collide with the tine frequency.

solution consisted of deionized water (15.3 MΩ cm resistivity) with a 1 molar solution of potassium hydroxide (KOH). Mass was removed from the probes in small increments (5–10 μg) and measured from the electrode charge transfer during etching (using chronocoulometry). Figure 5 shows the etching experimental setup. Voltage is applied across the carbon rods and the probe fiber. Current through this cell (i) is in series with a resistor (R_{ref}) that provides a voltage (V_R) that is amplified (by factor of G which generates V_O). This output voltage is then integrated to measure the amount of charge (q) from which mass removal is calculated. For the conditions of these experiments, 1 tungsten atom is removed for every 6 electrons through the cell. More details about the development of the etching instrument is presented in Ref. 20.

After shortening the length (or diameter) of the fibers, a lock-in amplifier is used to generate a frequency sweep to obtain the new frequency response of the probe.

IV. RESULTS

Results presented in this section illustrate the correlation between the two theoretical approaches with experimental data and FEA results. First, the result of two beams serially connected method, predicting the behavior of probes versus the fiber varying length and diameter compared with experimental data is represented. Next, the amplitude and phase frequency response of the probe obtained from

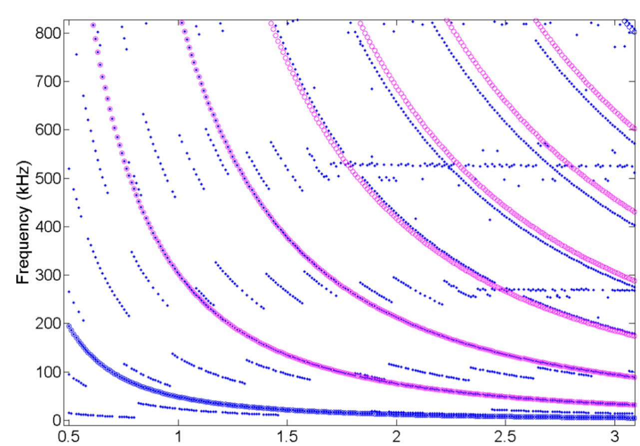

FIG. 8. Theoretical calculation of frequency as a function of length of fiber for first ten resonant modes obtained from theoretical model for two serially connected beams (tungsten probe).

TABLE V. Natural frequencies of tine obtained from theoretical calculation demonstrating its behavior acting as clamped-clamped beam.

Mode (r)	Natural frequencies, simulation (kHz)	$\frac{\omega_r}{\omega_1} = \frac{\alpha_r^2}{\alpha_1^2}$ for clamped-pinned beam	Natural frequencies, clamped-pinned beam (kHz)	$\frac{\omega_r}{\omega_1} = \frac{\alpha_r^2}{\alpha_1^2}$ for clamped-free beam	Natural frequencies, clamped-free beam (kHz)
f_1	20	1.0	20	1.0	20
f_2	100	3.24	64.8	6.26	125.2
f_3	275	6.76	135.2	17.54	350.8
f_4	530	11.56	231.2	34.38	687.6
f_5	875	17.64	352.8	56.84	1136.8

lumped absorption model is illustrated. Finally, the natural frequencies of probes and their modes shapes obtained from FEA simulation and the comparison with experimental data are provided.

A. Varying length

Figure 6 illustrates the first ten modes of the carbon probe obtained from the theory for lateral vibration of two beams serially connected, Section II A. In this figure the asymptotic loci of markers represented with blue dots show the modes of the probe which demonstrates the natural frequencies relationship with length of the fiber. The asymptotic lines represented with pink circles correspond closely to the natural frequencies for the carbon fiber modeled as a single cantilever beam. The consistency between these two lines indicates that the carbon probe is behaving similar to a cantilever beam.

Oscillation of carbon fiber with 7 μm diameter attached to tuning fork shows a clear illustration of modal frequencies. The photograph of these observations (obtained experimentally) for third, fourth, and fifth modes is shown in Figure 7 as an illustration.[21]

Figure 8 shows the frequency-fiber length plot for the tungsten probe. In this figure, the difference between lines with blue dots and pink circles is more significant than the one depicted in Figure 6. It is speculated that since the tungsten fiber has larger diameter and is heavier than the carbon fiber, it therefore results in the probe deviating further from simple cantilever type behavior. Generally, for "touch" sensitivity, the probe length is optimal when the fiber oscillates at maximum (or near to maximum) amplitude. This corresponds closely to the zeros in the frequency response plot. Not coincidentally, these are also located in a region where the probe, and closely related independent fiber, frequencies coincide closely to that of the independent tine first mode resonance. It might be expected that the fiber will have a node at the attachment point at the tip of the tine at which point it will act as an absorber. Consequently, under these combined favorable conditions, the energy supplied to the tine will be maximally transferred to the fiber that is typically excited in a much higher mode. For a simple cantilever, the maximum total potential, V, and kinetic energy, T, associated with oscillation of the fiber are

$$V = \frac{EI}{2l^3}\sum_{s=1}^{\infty}(\alpha\mu_s l)^4 q_s^2,$$
$$T = \frac{\rho A l}{2}\sum_{s=1}^{\infty}\dot{q}_s^2 = \left(\frac{EI}{2l^3}\right)\sum_{s=1}^{\infty}(\alpha\mu_s l)^4 q_s^2, \tag{23}$$

where q_s represents the modal (or normal) coordinate associated with the sth mode. In fact, under these optimal conditions, the fiber may be considered to be an optimal absorber for the tine.

Also shown in Figures 6 and 8 are eigenvalues of the matrix that, while exhibiting asymptotic behavior over short changes in length, these then jump to form a series of short segments that correspond to a nearly constant frequency. These lines correspond to the natural frequencies of the tuning

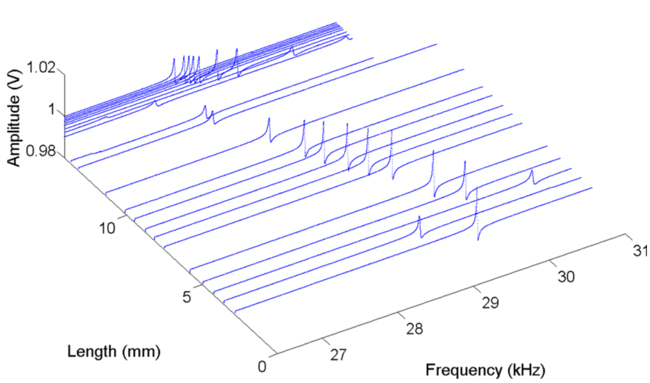

FIG. 9. Experimentally measured frequency response of a tungsten probe sequentially etched to different lengths.

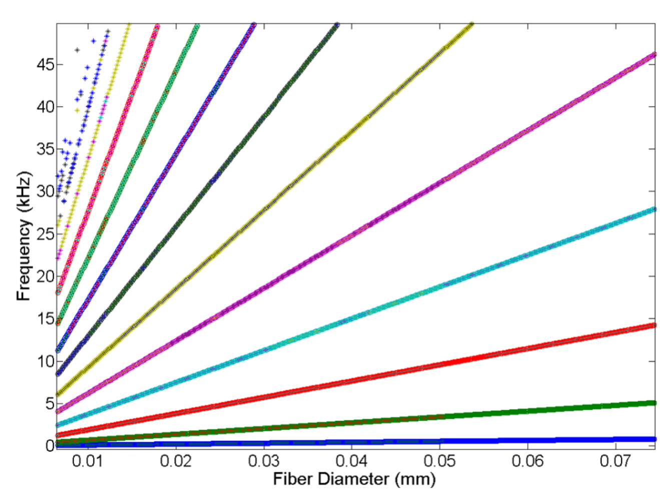

FIG. 10. Theoretical calculation of eigenvalues for an 8.16 mm long tungsten fiber as a function of varying diameter.

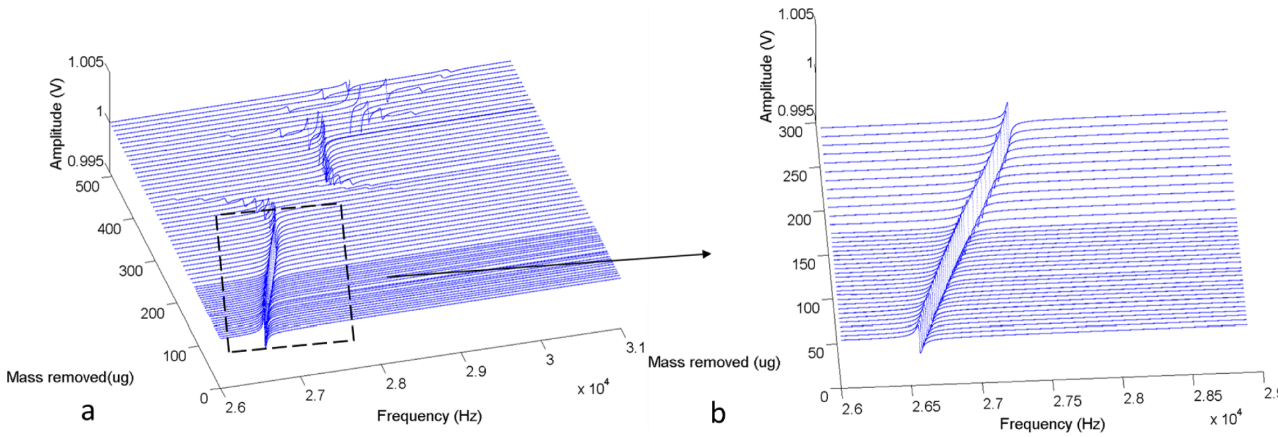

FIG. 11. (a) Frequency response of tungsten fiber obtained from experimental testing (b) subplot of 14-a demonstrating the linear relationship of modal frequencies with fiber diameter.

fork tine in different modes, for which four of them are highlighted in Figure 6. For the longer fiber lengths, values for the first five frequencies have been extracted from these theoretical plots, and the ratio between them is compared with different cantilever beam types, see Table V. The ratio of the modal frequencies shows that the tuning fork tine is behaving as beam with frequency being between clamped-pinned and clamped-free conditions. One side of the tine is assumed to be clamped as it is stated in the boundary condition (Equation (3)). The other end of the tine will experience varying dynamic forces that will depend on the free natural frequencies of both beams. For high frequencies, forces on the tine due to fiber mass and the second moment of mass will be relatively large, effectively acting to a pin the "free" end of the tine. For lower frequencies however, the effect of the fiber mass is less significant thus, the fiber forces at the end of the tine become less significant and it responds more closely to being free at the end.

Figure 9 shows the experimentally measured frequency response in terms of magnitude and frequency as a function of the length of the tungsten fiber. The initial length of the fiber used was 14.11 mm after which it was etched down to 0.83 mm in non-equal steps (due to difficulties associated with controlling the immersed length of the fiber tip in the electrolyte solution). It can be noticed that the natural frequencies of the probe at different modes are changing asymptotically with respect to the length of the fiber similar to the observations obtained from theoretical graphs in Figures 6 and 8. This will be further discussed in Section IV C.

B. Varying diameter

Another study has been carried out to examine the effect on probe's natural frequency of changing the fiber diameter. Figure 10 plots the theoretical eigenvalues for a tungsten fiber of length 8.16 mm attached to a tuning fork tine. Different colors in the graph show different modes of the probe and demonstrate a linear relationship with varying fiber diameter.

This can be predicted from the vibrating cantilever beam equations. The natural frequencies of a cantilever beam is obtained from

$$f_n = \frac{(\alpha_n l)^2}{2\pi}\sqrt{\frac{EI}{mL^3}}. \tag{24}$$

Substituting I and m for a cylindrical rod yields

$$f_n = \frac{(\alpha_n l)^2}{2\pi}\sqrt{\frac{E\left(\frac{\pi D^4}{64}\right)}{\left(\rho\frac{\pi D^2}{4}L\right)L^3}} = \frac{(\alpha_n l)^2 D}{8\pi L^2}\sqrt{\frac{E}{\rho}}. \tag{25}$$

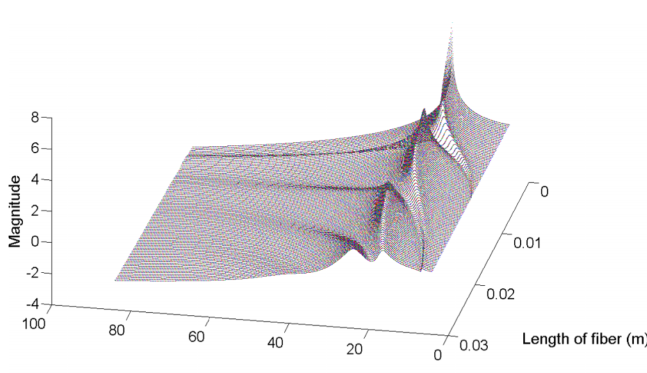

FIG. 12. Amplitude frequency response of the tuning fork tine, H_{oy} as a function of tungsten fiber length based on lumped model approximation (tungsten probe).

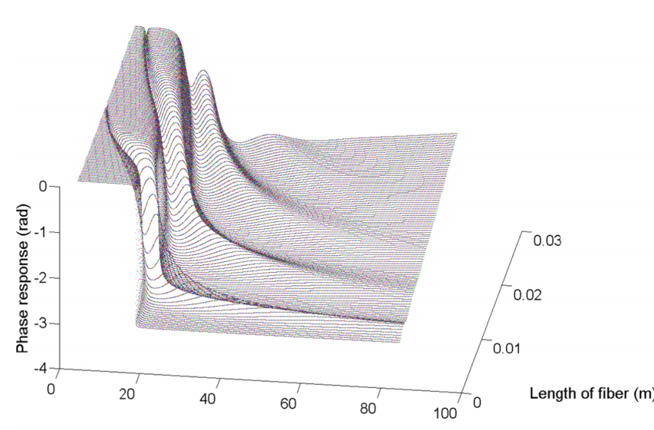

FIG. 13. Phase frequency response of the tuning fork tine as a function of attached tungsten fiber length based on lumped model approximation.

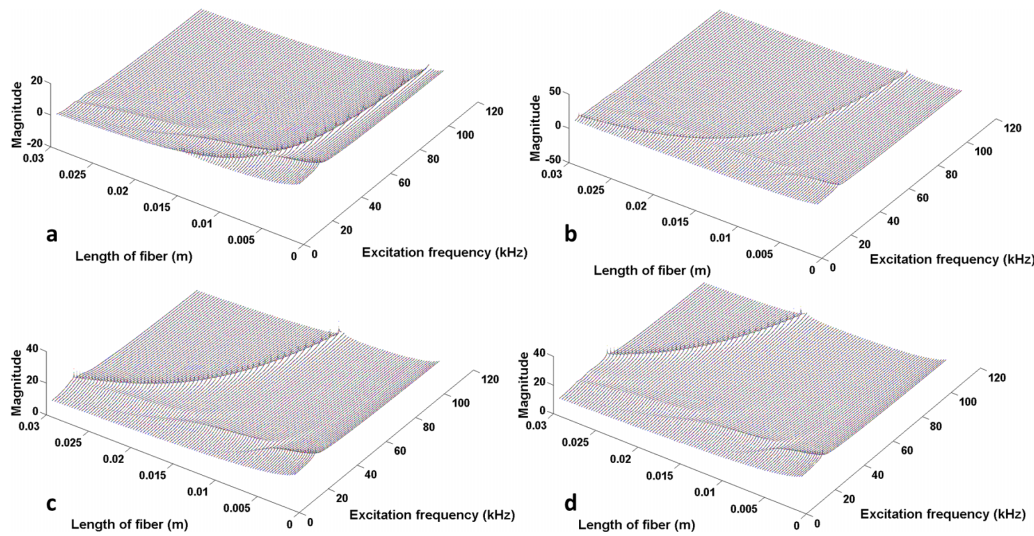

FIG. 14. Amplitude frequency response of the fiber, H_{iy} for $i = 1$, 2, 3, and 4, respectively, as a function of fiber length based on the lumped model approximation (tungsten probe).

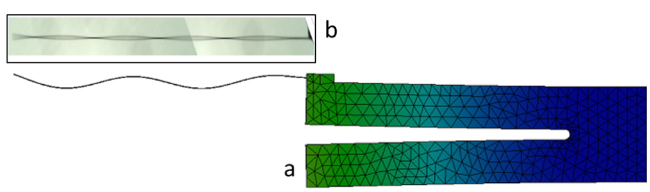

FIG. 15. Fifth oscillating mode shape of carbon probe of 4.3 mm fiber length obtained from (a) FEA, (b) experimental testing.

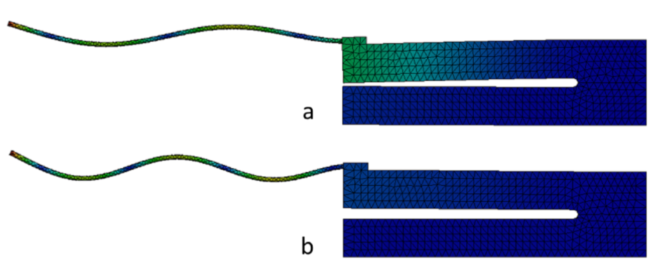

FIG. 16. FEA result showing modes shapes of tungsten probe of 5.5 mm fiber length oscillating in (a) third mode and (b) fourth mode.

Therefore, the natural frequency is expected to vary linearly with the diameter of the rod and hyperbolically with length. The result of the experimental test where a tungsten probe (8.16 mm long fiber attached to tuning fork) is etched in step of 5 μg (decreasing diameter) is shown in Figure 11.

C. Lumped system model

Figure 12 represents the amplitude frequency response plot showing the magnitude of H_{oy} (Equation (21)) as a function of length of a tungsten fiber of radius 37.5 μm.

The phase response of H_{oy} as a function of frequency and diameter is shown in Figure 13.

Similarly, the amplitude frequency response of individual lumped modes H_{iy} (Equation (22)) is plotted relative to the length of the fiber. These plots for the first four modes of a tungsten probe are shown in Figure 14. The same asymptotic lines represented in Figures 6 and 8 are noticeable in these images. Most significantly, and as expected from this lumped model approximation, the response for each fiber dominates while, because all coordinates of the system response share common roots, the influence of the surrounding system remains. However, it is apparent that the resonant peak for each fiber mode passes through the location of the zero in the tuning fork response.

TABLE VI. First five natural frequencies of the tungsten probe (fiber length = 5.5 mm) obtained from theoretical calculation and FEA.

Mode (r)	Natural frequencies, from theory (Hz)	Natural frequencies from FEA (Hz)
f_1	1 801.5	158 0
f_2	11 289.6	970 9
f_3	31 611.3	314 17
f_4	61 945.4	557 68
f_5	101 332.0	906 07

D. Finite element analysis

A frequency study using FEA software available in SolidWorks™ has been carried out on a 3D solid model of the probes. Figure 15 shows the fifth mode shape of the oscillating carbon probe acquired from FEA, and its consistency with the experimental image.

The third and fourth mode shapes of tungsten probe with 5.5 mm fiber length obtained from an FEA study are shown in Figure 16.

The natural frequencies of first five modes for tungsten probe (fiber length = 5.5 mm) acquired from theoretical calculation (two beams serially connected method) and FEA is represented in Table VI, which represent a good correlation between two approaches.

It is noted that the theoretical model predicts frequencies that are higher than of those obtained from FEA. Two possible sources of this difference are mesh size used and the fact that the fiber bonds a short distance on to the end of the tine. Consequently, the additional mass due to the short length of fiber on the end of the tine is not included in the theoretical model. Such a reduction in mass would be expected to result in higher natural frequencies.

V. CONCLUSIONS

Micro-scale oscillatory probes are widely used in metrology, manufacturing, and assembly for precision applications. Two beams serially connected and lumped model approximate vibration models are developed in this paper for detailed understanding of the dynamics of these probes.

Experiments have been carried out with tungsten and carbon probes where the fiber length or diameter was electrolytically etched and their frequency response was acquired. The results from theoretical models and the experimental data displayed natural frequencies of probes to retain an asymptotic relationship with the fiber length and a linear relationship with the fiber diameter. Additionally, the tuning forks in these probes can be modelled with eigenvalues varying between clamped-pinned and clamped-free beams that depend on how closely the fiber resonance (a function of the fiber length or diameter) coincides with that of the tine. Moreover, a frequency study in SolidWorks predicted the probe mode shapes and its natural frequencies which were consistent with the data obtained from experiments, hence it rules out the necessity of complex FEA studies.

A key functional characteristic of these probes is the matching of the fiber modes to that of the first mode of the tine. Generally, the electrode pattern on the tuning fork tines is designed to excite the fundamental mode. Consequently, this excitation shape is not suited for exciting other probe modes. When the frequencies of fiber modes that are not closely matched to that of the tine, even though they may independently have a relatively high Q value, the tine excitation, and therefore the fiber, will have a low amplitude. The approaching and receding fiber modes are visible in Figure 10 for tungsten fiber lengths at 3 mm and 13 mm. When the fiber length contains a mode close to the tine natural frequency, the energy of excitation is transferred into the fiber that then acts as an absorber for the tine mode, resulting in a zero for the frequency response of the tine (i.e., the frequency response that is measured by these types of probe).

While the focus of this study is the analysis of probes undergoing planar oscillations, in practice there are additional modes resulting in out-of-plane motion. Planar analysis is justified by the fact that the excitation force is applied only in this plane and that the results from both theory and experiment are consistent in terms of pole and zero locations in the probe response. Non-linear effects have been observed, more commonly occurring with high Q systems or those having measurable assembly errors such as misalignment between the axis of the fiber and that of the tine. Additionally, when these probes are used as contact sensors, the dynamics of the interaction is typically chaotic. Both of these topics, while interesting, are outside of the scope of this paper. However, there are applications for which multi-directional oscillators for contact sensing applications are of interest, particularly in the field of micrometer-scale touch-sensors for coordinate measuring machines.[22–25] It is expected that the technique for optimizing performance for the planar probe could be similarly determined for any resonant probe designs comprising slender elements attached to an oscillator operating at fundamental or higher modes.

While the probes of this study might oscillate in a single plane, the frequency response does change when the probe is brought into proximity with a surface having any orientation relative to the direction of oscillation. Studies to quantify this orientation dependence have yet to be undertaken. Additional studies are also necessary to determine the optimal parameters for probe designs in terms of subsequent signal sensitivity as a function of proximity to a specimen surface. Sensitivity is also complicated by the choice of excitation parameters (amplitude, frequency, and phase) in the region of the resonant peak. Studies to quantify these parameters are planned, ultimately aimed at achieving optimal performance in terms of bandwidth and signal to noise ratio of micro-resonator probes.

ACKNOWLEDGMENTS

This material is based upon work supported by the National Science Foundation (NSF) under Award Nos. DMI 1000656 and DMI 1538814. Any opinions, findings, and conclusions or recommendations expressed in this publication are those of the author(s) and do not necessarily reflect the views of the National Science Foundation. Furthermore, the authors would like to thank Dr. Bartosz Nowakowski for his help in the development of the electrolyte etching instrument and the Center for Precision Metrology (CPM) for providing facilities in fulfilling this project.

APPENDIX: EQUATIONS FOR GENERATING THE MATRIX GOVERNING MOTION

Dropping the s subscript, Equations (4) and (5) can be expressed in the form

$$\frac{y_1(x_1,q_1)}{q_1} = A_1\left(\cos(\beta\gamma\alpha_2 x_1) - \cosh(\beta\gamma\alpha_2 x_1)\right) + A_3\left(\sin(\beta\gamma\alpha_2 x_1) - \sinh(\beta\gamma\alpha_2 x_1)\right), \tag{A1}$$

$$\frac{y_2(x_2,q_2)}{q_2} = B_1 \cos(\alpha_2 x_2) + B_2 \cosh(\alpha_2 x_2) + B_3 \sin(\alpha_2 x_2) + B_4 \sinh(\alpha_2 x_2). \tag{A2}$$

Satisfying the rest of the boundary conditions is not as straightforward. Consider each of the conditions in Equation (3) in turn

$$y_1(L_1) = A_1(\cos(\beta\alpha_2 L_2) - \cosh(\beta\alpha_2 L_2)) + A_3(\sin(\beta\alpha_2 L_2) - \sinh(\beta\alpha_2 L_2)) = y_2(0) = B_1 + B_2, \tag{A3}$$

$$\frac{dy_1(L_1)}{dx_1} = A_1\beta\gamma\alpha_2(-\sin(\beta\alpha_2 L_2) - \sinh(\beta\alpha_2 L_2)) + A_3\beta\gamma\alpha_2(\cos(\beta\alpha_2 L_2) - \cosh(\beta\alpha_2 L_2)) = \frac{dy_2(0)}{dx_2} = B_3\alpha_2 + B_4\alpha_2, \tag{A4}$$

or

$$A_1\beta\gamma(-\sin(\beta\alpha_2 L_2) - \sinh(\beta\alpha_2 L_2)) + A_3\beta\gamma(\cos(\beta\alpha_2 L_2) - \cosh(\beta\alpha_2 L_2)) = B_3 + B_4,$$

$$E_1 I_1 \left.\frac{d^2 y_1}{dx_1^2}\right|_{x_1=L_1} = E_1 I_1(\beta\gamma\alpha_2)^2 \begin{bmatrix} -A_1(\cos(\beta\alpha_2 L_2) + \cosh(\beta\alpha_2 L_2))\ldots \\ \ldots - A_3(\sin(\beta\alpha_2 L_2) + \sinh(\beta\alpha_2 L_2)) \end{bmatrix} = E_2 I_2 \left.\frac{d^2 y_2}{dx_2^2}\right|_{x_2=0} = E_2 I_2 \alpha_2^2[-B_1 + B_2], \tag{A5}$$

or

$$E_1 I_1(\beta\gamma)^2 \begin{bmatrix} -A_1(\cos(\beta\alpha_2 L_2) + \cosh(\beta\alpha_2 L_2))\ldots \\ \ldots - A_3(\sin(\beta\alpha_2 L_2) + \sinh(\beta\alpha_2 L_2)) \end{bmatrix} = E_2 I_2[B_2 - B_1],$$

$$E_1 I_1 \left.\frac{d^3 y_1}{dx_1^3}\right|_{x_1=L_1} = E_1 I_1(\beta\gamma\alpha_2)^3 \begin{bmatrix} A_1(\sin(\beta\alpha_2 L_2) - \sinh(\beta\alpha_2 L_2))\ldots \\ \ldots A_3(-\cos(\beta\alpha_2 L_2) - \cosh(\beta\alpha_2 L_2)) \end{bmatrix} = E_2 I_2 \left.\frac{d^3 y_2}{dx_2^3}\right|_{x_2=0} = E_2 I_2 \alpha_2^3[-B_3 + B_4], \tag{A6}$$

or

$$E_1 I_1(\beta\gamma)^3 \begin{bmatrix} A_1(\sin(\beta\alpha_2 L_2) - \sinh(\beta\alpha_2 L_2))\ldots \\ \ldots A_3(-\cos(\beta\alpha_2 L_2) - \cosh(\beta\alpha_2 L_2)) \end{bmatrix} = E_2 I_2[-B_3 + B_4],$$

$$\frac{d^2 y_2(L_2)}{dx_2^2} = -B_1\alpha_2^2\cos(\alpha_2 L_2) + B_2\alpha_2^2\cosh(\alpha_2 L_2) - B_3\alpha_2^2\sin(\alpha_2 L_2) + B_4\alpha_2^2\sinh(\alpha_2 L_2) = 0,$$

$$\frac{d^3 y_2(L_2)}{dx_2^3} = B_1\alpha_2^3\sin(\alpha_2 L_2) + B_2\alpha_2^3\sinh(\alpha_2 L_2) - B_3\alpha_2^3\cos(\alpha_2 L_2) + B_4\alpha_2^3\cosh(\alpha_2 L_2) = 0, \tag{A7}$$

or

$$-B_1\cos(\alpha_2 L_2) + B_2\cosh(\alpha_2 L_2) - B_3\sin(\alpha_2 L_2) + B_4\sinh(\alpha_2 L_2) = 0,$$
$$B_1\sin(\alpha_2 L_2) + B_2\sinh(\alpha_2 L_2) - B_3\cos(\alpha_2 L_2) + B_4\cosh(\alpha_2 L_2) = 0.$$

Equations (A3)–(A7) are combined and written in a matrix form which represents the matrix governing motion of the system. The eigenvalues of this matrix are the natural frequencies of the probe.

[1] J. E. Sader, I. Larson, P. Mulvaney, and L. R. White, "Method for the calibration of atomic force microscope cantilevers," Rev. Sci. Instrum. **66**, 3789 (1995).
[2] J. E. Sader, J. W. M. Chon, and P. Mulvaney, "Calibration of rectangular atomic force microscope cantilevers," Rev. Sci. Instrum. **70**, 3967 (1999).
[3] K. Karrai and R. D. Grober, "Piezoelectric tip-sample distance control for near field optical microscopes," Appl. Phys. Lett. **66**, 1842 (1995).
[4] J. C. Brice, "Crystals for quartz resonators," Rev. Mod. Phys. **57**, 105–146 (1985).
[5] M. Torralba, D. J. Hastings, J. D. Thousand, B. K. Nowakowski, and S. T. Smith, "A three-fingered, touch-sensitive, metrological micro-robotic assembly tool," Meas. Sci. Technol. **26**, 125902 (2015).
[6] M. B. Bauza, R. J. Hocken, S. T. Smith, and S. C. Woody, "Development of a virtual probe tip with an application to high aspect ratio microscale features," Rev. Sci. Instrum. **76**, 095112 (2005).
[7] S. Woody, B. Nowakowski, M. Bauza, and S. T. Smith, "Standing wave probes for microassembly," Rev. Sci. Instrum. **79**, 085107 (2008).
[8] C. Gabrielli, "Calibration of the electrochemical quartz crystal microbalance," J. Electrochem. Soc. **138**, 2657 (1991).
[9] S.C. Howard, J. W. Chesna, S. T. Smith, and B. A. Mullany, "On the development of an experimental testing platform for the vortex machining process," J. Manuf. Sci. Eng. **135**, 051005 (2013).
[10] S. C. Howard, J. W. Chesna, B. A. Mullany, and S. T. Smith, "Observations during vortex machining process development," in *ASME 2012 International Manufacturing Science and Engineering Conference* (ASME, 2012), p. 25.
[11] B. K. Nowakowski, S. T. Smith, B. A. Mullany, and S. C. Woody, "Vortex machining: Localized surface modification using an oscillating fiber probe," Mach. Sci. Technol. **13**, 561–570 (2009).
[12] H. Qi, "High Speed Motion Generated by an Oscillating Microfiber," M.Sc. thesis (Brown University, 2010).
[13] K. Chong, S. D. Kelly, S. T. Smith, and J. D. Eldredge, "Inertial particle trapping in viscous streaming," Phys. Fluids **25**, 033602 (2013).
[14] S. Kafashi, J. Eldredge, S. Kelly, and S. T. Smith, "Microscopic-based imaging for precision measurement of micro scale flows around dynamically oscillating objects," in *Proceedings - ASPE 2015 Annual Meeting* (ASPE, 2015), Vol. 62, pp. 336–341.
[15] S. Kafashi, J. Eldredge, K. Chong, J. D. Thousand, S. Kelly, and S. T. Smith, "Development of experimental facilities for investigations of microscopic mapping of fluid velocities," in *Proceedings - ASPE 2014 Annual Meeting* (ASPE, 2014), Vol. 59, pp. 302–306.

[16] K. Chong, S. D. Kelly, S. T. Smith, and J. D. Eldredge, "Transport of inertial particles by viscous streaming in arrays of oscillating probes," Phys. Rev. E **93**, 013109 (2016).
[17] R. E. D. Bishop and D. C. Johnson, *The Mechanics of Vibration* (Cambridge University Press, 1979).
[18] J. W. S. Rayleigh, *The Theory of Sound* (Macmillan, 1894), Vol. 1.
[19] S. T. Smith, *Flexures: Elements of Elastic Mechanisms* (CRC Press, 2000).
[20] B. K. Nowakowski, S. T. Smith, J. R. Pratt, and G. A. Shaw, "Chronocoulometry for quantitative control of mass removal in micro-structures and sensors," Rev. Sci. Instrum. **83**, 105115 (2012).
[21] J. B. Hunt, "Experimental Investigation of Process Parameters in Vortex Machining," M.Sc. thesis (University of North Carolina at Charlotte, 2014).
[22] J. D. Claverley and R. K. Leach, "Development of a three-dimensional vibrating tactile probe for miniature CMMs," Precis. Eng. **37**, 491–499 (2013).
[23] J. D. Claverley and R. K. Leach, "A vibrating micro-scale CMM probe for measuring high aspect ratio structures," Microsyst. Technol. **16**, 1507–1512 (2009).
[24] H. Haitjema, W. O. Pril, and P. H. J. Schellekens, "Development of a silicon-based nanoprobe system for 3-D measurements," CIRP Ann. - Manuf. Technol. **50**, 365–368 (2001).
[25] S. C. Woody and S. T. Smith, "Resonance-based vector touch sensors," Precis. Eng. **27**, 221–233 (2003).